

IE2Video: Adapting Pretrained Diffusion Models for Event-Based Video Reconstruction

Dmitrii Torbunov¹, Onur Okuducu¹, Yi Huang¹, Odera Dim¹, Rebecca Coles¹,
Yonggang Cui¹, Yihui Ren¹,

¹Brookhaven National Laboratory, Upton, NY, USA

{dtorbunov, ookuducu, yhuang2, dodera, rcoles, ycui, yren}@bnl.gov

Abstract

Continuous video monitoring in surveillance, robotics, and wearable systems faces a fundamental power constraint: conventional RGB cameras consume substantial energy through fixed-rate capture. Event cameras offer sparse, motion-driven sensing with low power consumption, but produce asynchronous event streams rather than RGB video. We propose a hybrid capture paradigm that records sparse RGB keyframes alongside continuous event streams, then reconstructs full RGB video offline—reducing capture power consumption while maintaining standard video output for downstream applications. We introduce the Image and Event to Video (IE2Video) task: reconstructing RGB video sequences from a single initial frame and subsequent event camera data. We investigate two architectural strategies: adapting an autoregressive model (HyperE2VID) for RGB generation, and injecting event representations into a pretrained text-to-video diffusion model (LTX) via learned encoders and low-rank adaptation. Our experiments demonstrate that the diffusion-based approach achieves 33% better perceptual quality than the autoregressive baseline (0.283 vs 0.422 LPIPS). We validate our approach across three event camera datasets (BS-ERGB, HS-ERGB far/close) at varying sequence lengths (32–128 frames), demonstrating robust cross-dataset generalization with strong performance on unseen capture configurations.

1. Introduction

Video capture has become ubiquitous across applications ranging from surveillance and autonomous navigation to mobile devices and Internet-of-Things systems. However, continuous RGB video recording remains power-intensive, creating a fundamental bottleneck for battery-operated deployments. Modern RGB cameras require constant power

to capture frames at fixed temporal intervals, leading to prohibitive energy consumption in always-on scenarios where video must be recorded continuously over extended periods.

Event cameras offer a fundamentally different sensing paradigm. Unlike conventional frame-based sensors that capture images synchronously at fixed rates, event cameras are asynchronous sensors that respond to per-pixel brightness changes, outputting a sparse stream of events only when motion occurs in the scene [5]. This adaptive sampling strategy, which measures visual information based on scene dynamics rather than a fixed clock, provides several key advantages: microsecond-level temporal resolution, high dynamic range (140 dB compared to 60 dB for standard cameras), and low power consumption. These properties make event cameras particularly attractive for robotics and wearable applications operating under challenging conditions.

However, event cameras produce asynchronous event streams rather than RGB video. This creates a mismatch for applications that require standard video output—many existing systems, user interfaces, and archival workflows are designed around dense RGB video rather than sparse event data.

We explore a hybrid capture paradigm: capture sparse RGB keyframes alongside a continuous event stream, then computationally reconstruct full RGB video offline. This approach offers dual benefits. First, it reduces power consumption during capture by minimizing RGB sensor activity while relying on the event camera’s efficient motion sensing. Second, it provides storage efficiency for scenarios with intermittent motion—static scenes generate minimal event data, while dynamic scenes produce sparse events that compactly represent motion information. The reconstruction occurs offline, where power and computational resources are less constrained, enabling high-quality video generation from the captured sparse representation.

In this work, we introduce the Image and Event to Video (IE2Video) task: reconstructing a full RGB video from a

single initial frame and subsequent event stream (Figure 1). While related problems have been explored in the literature, none directly address this specific formulation. Frame interpolation methods [3, 8, 25, 26] operate on multiple uniformly-sampled RGB frames but are typically limited to interpolating only a few intermediate frames (1–3) between keyframes, making them unsuitable for generating long sequences from a single frame. Event-based reconstruction methods [4, 17, 20, 23, 29] have focused primarily on intensity-only image generation or very short sequences.

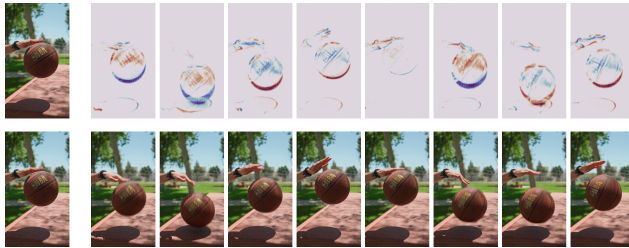


Figure 1. Task: RGB video reconstruction from a keyframe and sparse event camera data. Given only the first RGB frame (leftmost, shared between rows) and event camera stream (top row showing motion-encoded brightness changes), the goal is to generate a full RGB video sequence matching the ground truth frames (bottom row).

To address this challenge, we explore two architectural approaches for RGB video generation from sparse keyframes and events. We begin by adapting the widely successful HyperE2VID architecture [4], an autoregressive model originally designed for event-based intensity reconstruction, to our RGB video generation task. While this approach demonstrates capability in reconstructing moving objects, it struggles to maintain consistent backgrounds across longer sequences. Given the recent success of pretrained video generative models in domain adaptation tasks [27, 31], we investigate an alternative approach: injecting event information into a pretrained text-to-video generative model (LTX [7]) via learned event encoders and low-rank transformer adaptation. We compare these two architectural paradigms across multiple datasets and analyze their respective strengths through extensive ablations.

Our experiments demonstrate that the diffusion-based approach achieves 33% better perceptual quality than the autoregressive baseline (0.283 vs. 0.422 LPIPS) and maintains strong performance when evaluated across three event camera datasets at varying sequence lengths (32–128 frames).

The main contributions of this work are:

- We introduce the Image and Event to Video (IE2Video) task: generating RGB video sequences from sparse RGB keyframes and event camera data for power-efficient video capture.
- We demonstrate that adapting pretrained text-to-video

diffusion models via event injection outperforms end-to-end trained autoregressive approaches by 33%, establishing the effectiveness of leveraging pretrained models for event-to-RGB video generation.

- We validate our approach across three event camera datasets (BS-ERGB, HS-ERGB far/close) at varying sequence lengths (32–128 frames), demonstrating robust cross-dataset generalization and temporal extrapolation beyond training length.

2. Related Work

2.1. Event-Based Reconstruction and Interpolation

Event cameras asynchronously capture per-pixel brightness changes, providing microsecond temporal resolution and high dynamic range [5]. Several methods reconstruct intensity images from event streams using recurrent architectures. E2VID [17] introduced a recurrent encoder-decoder that converts event representations into grayscale intensity frames, while subsequent works reduced model complexity [20] and improved reconstruction quality through hypernetwork-based adaptive filtering [4]. HyperE2VID [4], which we adapt as our autoregressive baseline, employs ConvLSTM layers [21] and dynamic convolutions [6] to generate temporally consistent intensity reconstructions from event streams. Recent methods have extended to RGB reconstruction, though typically limited to very short sequences (1–3 frames) [28].

A parallel line of work leverages events for frame interpolation. Event-based video frame interpolation (E-VFI) methods condition on two RGB keyframes and the intervening event stream to synthesize intermediate frames [25, 26]. Recent work has explored diffusion models for E-VFI, adapting pretrained video models through event-based motion control [3] or unsupervised cycle-consistent training [8].

However, existing work addresses fundamentally different problem formulations than ours. Event reconstruction methods focus on intensity-only (grayscale) output rather than RGB video, and typically generate very short sequences. E-VFI methods perform interpolation between densely-sampled keyframes (typically 1–3 intermediate frames), whereas our task requires extrapolating long sequences (32–128 frames) from a single initial frame. No prior work addresses RGB video generation from a single keyframe and event stream—the problem we introduce in this work.

2.2. Video Diffusion Models and Adaptation

Diffusion models have achieved strong results in video generation through iterative denoising processes [10, 18]. Recent video diffusion models employ transformer architectures and latent representations for efficient high-resolution

synthesis [1, 7]. These pretrained models encode strong temporal priors and motion understanding from large-scale video data.

Adapting pretrained models to new conditioning modalities has proven effective across various domains. ControlNet [34] introduced auxiliary networks for spatial conditioning in image diffusion, while recent work has extended conditioning mechanisms to video generation [14]. Parameter-efficient adaptation techniques such as Low-Rank Adaptation (LoRA) [11] enable fine-tuning large models with minimal trainable parameters.

We leverage these techniques to adapt LTX [7], a pretrained image and text-to-video model, for event camera conditioning. Our approach combines an event encoder with direct feature injection into the transformer backbone, using LoRA for parameter-efficient adaptation. The architectural details are described in [Section 3](#).

3. Methods

In this section, we formalize the problem setup ([Section 3.1](#)), then describe two architectural approaches: an autoregressive baseline inspired by event-based reconstruction methods ([Section 3.2](#)), and our primary contribution—a diffusion-based approach with event injection ([Section 3.3](#)).

3.1. Problem Formulation

We denote the initial RGB frame as $\mathbf{I}_0 \in \mathbb{R}^{3 \times H \times W}$ and the event stream as $\mathcal{E} = \{e_k\}_{k=1}^N$, where each event $e_k = (x_k, y_k, t_k, p_k)$ encodes the pixel location (x_k, y_k) , timestamp t_k , and polarity $p_k \in \{-1, +1\}$ indicating brightness increase (positive) or decrease (negative). Our objective is to generate a dense RGB video sequence $\mathbf{V} = \{\mathbf{I}_1, \mathbf{I}_2, \dots, \mathbf{I}_T\}$ of T frames, where each $\mathbf{I}_t \in \mathbb{R}^{3 \times H \times W}$ maintains photometric consistency with the initial frame and temporal consistency with the event-encoded motion.

To enable efficient neural network processing of the asynchronous event stream, we adopt the stacked temporal histogram representation from HyperE2VID [4]. We accumulate events \mathcal{E} spanning a temporal window ΔT (the interval between consecutive generated frames) into $B = 5$ temporal bins with differential polarity encoding:

$$\mathbf{F}_{\text{event}}(b, y, x) = \sum_{e \in \mathcal{E}} p_e \cdot \delta_x^{x_e} \delta_y^{y_e} \mathbf{1}_{[t_b, t_{b+1})}(t_e) \quad (1)$$

where $e = (x_e, y_e, t_e, p_e)$ denotes an event with spatial coordinates (x_e, y_e) , timestamp t_e , and polarity $p_e \in \{-1, +1\}$; $b \in \{0, \dots, B - 1\}$ is the temporal bin index with boundaries $t_b = b \cdot \Delta T / B$; and $\delta, \mathbf{1}$ denote the Kronecker delta and indicator function respectively. This yields an event frame $\mathbf{F}_{\text{event}} \in \mathbb{R}^{B \times H \times W}$, which is used for both our autoregressive and diffusion-based approaches.

3.2. Autoregressive Approach

We first explore an autoregressive architecture for RGB video generation from events. Autoregressive models are a natural baseline, having demonstrated strong performance in event-based intensity reconstruction. We adapt the state-of-the-art HyperE2VID architecture [4], originally designed for intensity reconstruction from pure event streams, to our task of RGB video generation conditioned on an initial frame.

Architecture. The HyperE2VID architecture employs an encoder-decoder structure with ConvLSTM recurrent layers [21] and dynamic convolutions generated via hypernetworks [6]. It takes two inputs: the event frame representation $\mathbf{F}_{\text{event}}^{(t)}$ and the previous reconstruction (initialized with \mathbf{I}_0 at $t = 0$), which are fused through a context fusion module.

We modify HyperE2VID in two key ways: (i) initializing with the provided RGB frame \mathbf{I}_0 instead of zeros to supply appearance and color information, and (ii) modifying the output layer to produce 3-channel RGB frames instead of single-channel intensity. The context fusion module correspondingly processes 3-channel reconstructions alongside the 5-channel event representation.

The model generates frames autoregressively: at timestep t , it consumes the event frame $\mathbf{F}_{\text{event}}^{(t)}$ and the previous reconstruction, producing the next frame in the sequence. The ConvLSTM layers maintain hidden states across timesteps, enabling temporal information accumulation throughout sequence generation.

Training. HyperE2VID is trained using a combination of perceptual and temporal consistency losses:

$$\mathcal{L}_{\text{total}} = \lambda_{\text{perc}} \mathcal{L}_{\text{LPIPS}} + \lambda_{\text{flow}} \mathcal{L}_{\text{flow}} \quad (2)$$

where $\mathcal{L}_{\text{LPIPS}}$ is the learned perceptual loss [35] with AlexNet backbone, and $\mathcal{L}_{\text{flow}}$ is the optical flow consistency loss [17].

Following the original HyperE2VID training strategy, we employ Truncated Backpropagation Through Time (TBPTT) [30] and curriculum learning with teacher forcing annealed. The complete training details are provided in the supplementary materials.

3.3. Adapting Pretrained Video Generation Models

While the autoregressive approach demonstrates promising capability in reconstructing dynamic objects, we observe limitations in maintaining consistent backgrounds across longer sequences—a known challenge for recurrent architectures in long-horizon generation tasks. Recent work has demonstrated that pretrained video generation models can be successfully adapted to new domains and conditioning modalities through parameter-efficient fine-tuning [12, 27, 31]. These models benefit from large-scale pretraining on

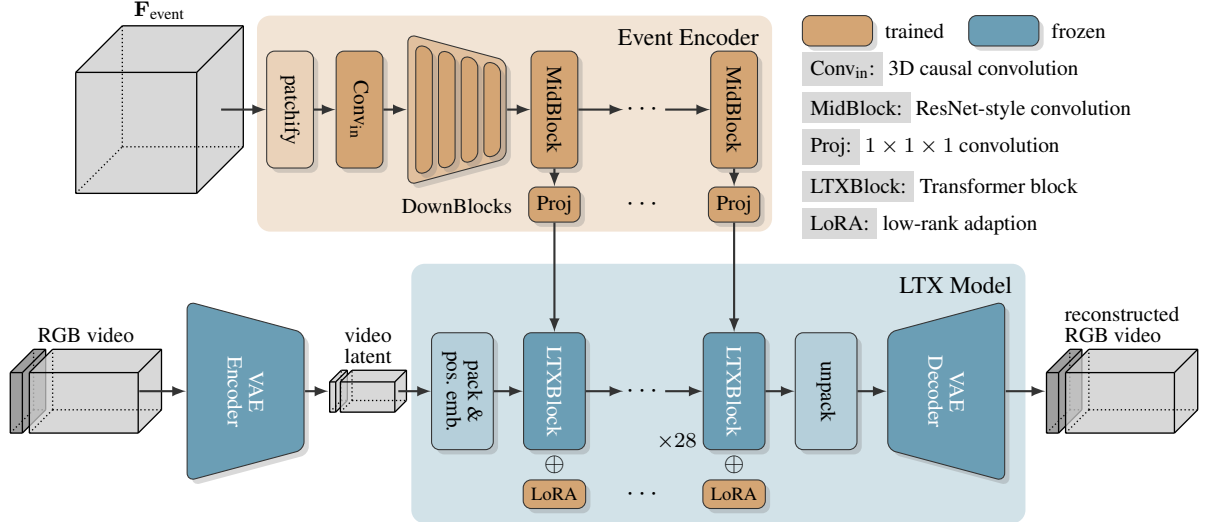


Figure 2. **LTX-Events architecture.** The video generation is trained by injecting encoded event information into the Transformer stack of the denoise decoder of pretrained LTX.

natural videos, providing strong priors for temporal coherence and motion dynamics.

Motivated by these observations, we explore adapting LTX [7], a pretrained text-and-image-to-video generation model, for event camera conditioning. The key technical challenge is determining how to inject event information into the pretrained architecture while preserving learned temporal coherence priors. In the following subsections, we describe our event conditioning mechanism (Section 3.3.2) and training procedure (Section 3.3.3). The network architecture is illustrated in Figure 2.

3.3.1. Base Architecture: LTX Video Generation Model

We build upon LTX-Video [7], a pretrained text-and-image-to-video generation model with 1.9 billion parameters. LTX employs a rectified flow formulation [13] for the generative process, which operates on a highly compressed latent space produced by a specialized video variational autoencoder (VAE). The core generative model follows a diffusion Transformer (DiT)-style architecture [2, 16], comprising 28 transformer blocks with a hidden dimension of 2048.

We select LTX for several practical reasons. First, its compact size (1.9B parameters) compared to alternative video generation models (typically 10B+ parameters [16, 32]) makes it feasible to fine-tune on limited compute resources—the model can be adapted on a single GPU with parameter-efficient methods, enabling rapid exploration of different conditioning mechanisms. Second, the aggressive latent compression reduces memory requirements and enables efficient attention over long sequences, which is critical for our 32–128 frame generation task. The model’s RoPE-based positional encoding allows the generation of arbitrary-length videos without requiring matched

training and inference sequence lengths, providing flexibility for future extensions to longer sequences. Finally, LTX achieves efficient inference, generating 5 seconds of video at 24 fps in approximately 2 seconds on an H100 GPU with 20 rectified flow steps [7, 13], facilitating rapid iteration during development.

3.3.2. Event Conditioning

A key challenge in adapting LTX for event conditioning is determining how to inject event information into the pretrained architecture while preserving the temporal coherence priors learned during pretraining. Recent work on event-based frame interpolation [3] has employed ControlNet-style conditioning [34] to inject event camera data into Stable Video Diffusion (SVD) [1], a pretrained video generation model. However, this approach exploits the encoder-decoder asymmetry inherent to SVD’s U-Net architecture [19], where ControlNet’s parallel encoder naturally mirrors the downsampling pathway and injects features via skip connections. In contrast, LTX employs a uniform DiT-style transformer architecture [15] with no encoder-decoder distinction—applying ControlNet to transformers would require duplicating the entire 1.9B parameter model, effectively training a parallel transformer rather than a lightweight conditioning module.

Given this architectural constraint, we adopt a direct *additive injection* strategy that leverages LTX’s uniform structure. Our approach consists of two components: an event encoder that processes event histogram representations into latent features compatible with LTX’s transformer, and an injection mechanism that integrates these features at each of the 28 transformer layers.

Event Encoder Architecture. The event encoder takes as input the event histogram representation $\mathbf{F}_{\text{event}} \in \mathbb{R}^{B \times H \times W}$ (defined in Section 3.1) and produces event-conditioned features $\mathbf{z}_{\text{event}} = \{\mathbf{z}_{\text{event}}^{(j)} \mid j = 1, \dots, 28\}$, one for each of LTX’s transformer blocks. We adopt an FPN-style architecture inspired by LTX’s video VAE encoder, which ensures compatibility with the latent space structure while enabling hierarchical feature extraction.

The encoder processes features through three stages. First, the input is patchified with a spatial patch of size 4 and processed by an initial causal 3D convolution [22]:

$$\mathbf{f}^{(0)} = \text{Conv}_{\text{in}}(\text{Patchify}(\mathbf{F}_{\text{event}})) \quad (3)$$

Second, a series of N_{down} downsampling blocks with ResNet-style 3D convolutions progressively reduce spatial resolution while increasing channel capacity, applying $32 \times$ spatial downsampling and $8 \times$ temporal downsampling:

$$\mathbf{f}^{(i)} = \text{DownBlock}^{(i)}(\mathbf{f}^{(i-1)}), \quad i \in \{1, \dots, N_{\text{down}}\} \quad (4)$$

The resulting bottleneck features contain 512 channels. Third, 28 ResNet-style 3D mid-level processing blocks refine these features and produce control signals via learned projections:

$$\mathbf{g}^{(j)} = \text{MidBlock}^{(j)}(\mathbf{g}^{(j-1)}), \quad j \in \{1, \dots, 28\} \quad (5)$$

$$\mathbf{z}_{\text{event}}^{(j)} = \text{Proj}^{(j)}(\mathbf{g}^{(j)}) \quad (6)$$

where $\mathbf{g}^{(0)} = \mathbf{f}^{(N_{\text{down}})}$ denotes the bottleneck features, and each projection $\text{Proj}^{(j)}$ is a $1 \times 1 \times 1$ convolution that maps from 512 to 2048 channels.

Following common practice in adapting pretrained models [34], we initialize all output projection layers with zero weights and biases. Full architectural details are provided in the supplementary material.

Injection Mechanism. Given the event-encoded features $\mathbf{z}_{\text{event}}$ from the encoder, we integrate them into LTX’s transformer via direct addition at each layer. Rather than hard-coding a specific integration mechanism (e.g., gated fusion, cross-attention, etc.), we provide event features directly to each transformer block and rely on learned adaptation (via LoRA, described below) to determine how each layer should leverage event information. Specifically, we modify the forward pass as:

$$\mathbf{h}^{(j)} = \text{LTXBlock}^{(j)}\left(\mathbf{h}^{(j-1)} + \mathbf{z}_{\text{event}}^{(j)}, \mathbf{c}_{\text{text}}\right), \quad j \in \{1, \dots, 28\} \quad (7)$$

where $\mathbf{h}^{(j)}$ denotes the hidden states after block j , and \mathbf{c}_{text} represents text conditioning (which we do not use in our

task). The event features are added to the hidden states *before* each transformer block processes them, allowing the block’s self-attention and feed-forward layers to integrate event information with the evolving video representation. By injecting at all 28 layers, we enable each transformer block to modulate its processing based on event information. We systematically ablate this design choice in Section 4 to determine which injection locations are most critical.

Parameter-Efficient Adaptation with LoRA. While the event encoder provides conditioning signals and direct addition makes them available to each transformer layer, the pre-trained LTX transformer must learn how to leverage these signals effectively. Full fine-tuning of the 1.9B parameter transformer risks catastrophic forgetting and requires substantial computational resources. Instead, we employ Low-Rank Adaptation (LoRA) [11], which introduces trainable low-rank decomposition matrices into the transformer’s linear layers while keeping the pretrained weights frozen.

3.3.3. Training Procedure

We train our model using the rectified flow objective [13], which learns a vector field that transports noise to data. Given ground truth latent representations \mathbf{x}_0 (encoded via LTX’s VAE) and noise $\epsilon \sim \mathcal{N}(\mathbf{0}, \mathbf{I})$, we compute the noised latent via linear interpolation $\mathbf{x}_\sigma = (1 - \sigma)\mathbf{x}_0 + \sigma\epsilon$ where $\sigma \sim \mathcal{U}[0, 1]$. The target velocity is $\mathbf{v}_{\text{target}} = \epsilon - \mathbf{x}_0$. To preserve first-frame conditioning, we apply minimal noise to initial frame tokens and exclude them from the loss via mask $\mathcal{M} \in \{0, 1\}^L$:

$$\mathcal{L}_{\text{RF}} = \mathbb{E}_{\sigma, \mathbf{x}_0, \epsilon} \left[\frac{1}{\|\mathcal{M}\|_1} \|\mathcal{M} \odot \mathbf{v}_{\text{diff}}\|^2 \right] \quad (8)$$

where $\mathbf{v}_{\text{diff}} = v_\theta(\mathbf{x}_\sigma, \sigma, \mathbf{z}_{\text{event}}) - \mathbf{v}_{\text{target}}$ and v_θ is the velocity prediction network (LTX transformer with LoRA adaptation and event injection).

4. Experiments and Results

4.1. Experimental Setup

Datasets. We train on the BS-ERGB dataset [26], which provides spatially-aligned event-RGB pairs captured with a beam splitter configuration. The dataset contains diverse dynamic scenes with complex motion patterns. We use the standard train/test split.

To assess cross-dataset generalization, we evaluate on HS-ERGB [25], which differs in capture hardware, frame rates, and scene characteristics. HS-ERGB provides two settings: *close planar sequences* with dynamic objects and non-linear motion, and *far-away sequences* with camera ego-motion at long depths. Evaluating on HS-ERGB without training demonstrates robustness to unseen capture configurations.

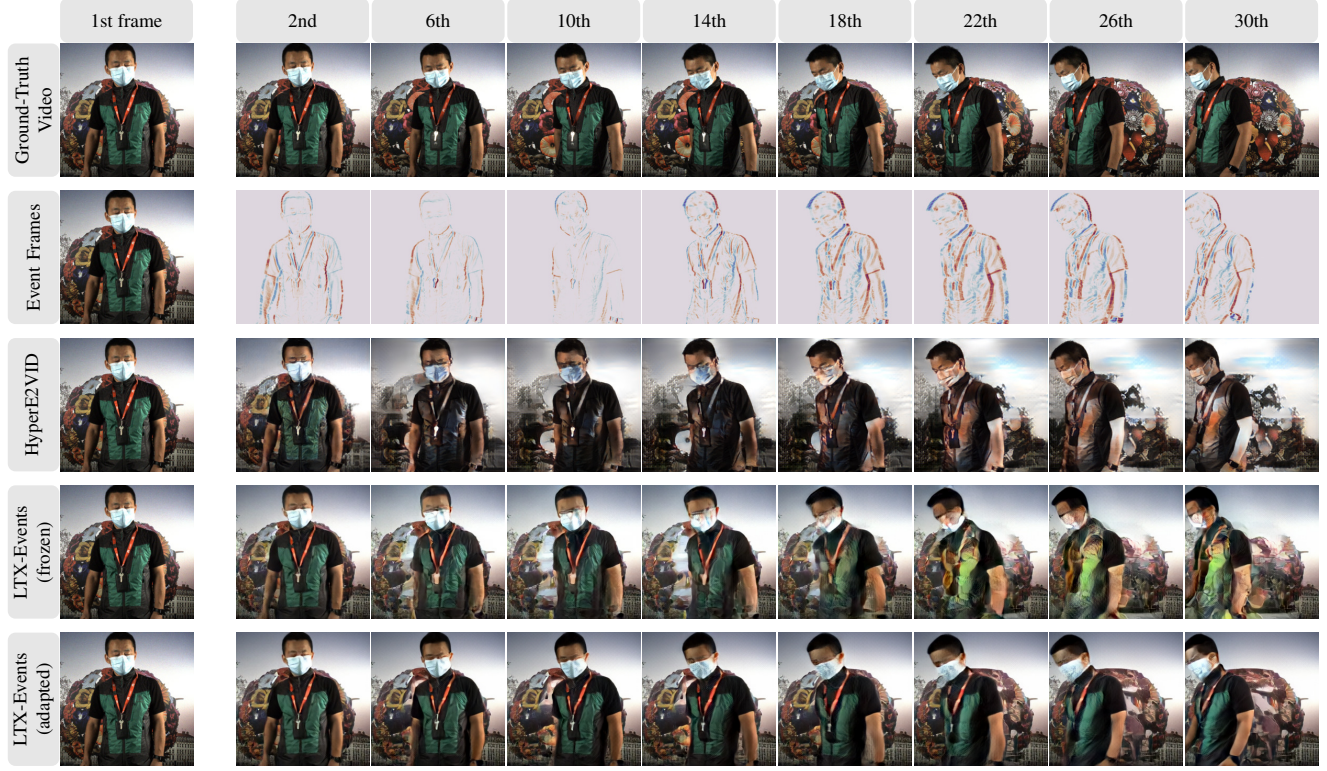


Figure 3. Qualitative comparison on BS-ERGB.

Evaluation Metrics. We use LPIPS [35] as our primary perceptual quality metric. We additionally report PSNR and SSIM as supplementary metrics for completeness. All metrics are computed on RGB frames at 256×256 resolution.

Implementation Details. We train all diffusion-based models for 400 epochs with batch size 4 on sequences of 32 frames at 256×256 resolution. We use the AdamW optimizer with learning rate 10^{-4} and default LoRA rank 32. For the autoregressive baseline (Section 3.2), we train for 400 epochs with curriculum learning (teacher forcing linearly annealed over the first 100 epochs), batch size 10, and sequences of 40 frames at 256×256 resolution. The complete training details are provided in the Supplementary Material.

At inference time, we generate videos of varying lengths (32, 64, or 128 frames) to test temporal extrapolation beyond the training sequence length. For diffusion models, we use 50 rectified flow steps. The autoregressive baseline naturally handles arbitrary-length generation through its recurrent structure.

Baselines. We compare against our autoregressive approach (Section 3.2), which adapts HyperE2VID [4] to RGB video generation conditioned on an initial frame. Our task formulation differs from frame interpolation (multiple keyframes) and event-only reconstruction (intensity, short sequences), making direct comparison to existing methods

infeasible.

4.2. Main Results

Table 1 compares our event-conditioned LTX approach against the HyperE2VID autoregressive baseline across three datasets and sequence lengths. We evaluate two variants: “frozen” (LoRA rank 0) trains only the event encoder, while “adapted” (LoRA rank 32) additionally adapts the transformer. All models train on sequences of 32–40 frames and evaluate at 32, 64, and 128 frames to assess temporal extrapolation.

Architectural comparison. Our adapted approach substantially outperforms the autoregressive baseline: 0.283 vs. 0.422 LPIPS at 32 frames on BS-ERGB (33% improvement), with similar gains on HS-ERGB close (0.231 vs. 0.530) and far (0.275 vs. 0.491). Improvements are consistent across PSNR and SSIM. While HyperE2VID performs reasonably at the training length, leveraging a pre-trained video generation model yields substantial improvements across all evaluation settings.

Necessity of transformer adaptation. Comparing frozen and adapted variants reveals that transformer adaptation is essential and becomes increasingly critical at longer sequences. At 32 frames, the frozen model achieves 0.345 LPIPS—better than HyperE2VID (0.422) but 18% worse than adapted (0.283). This gap widens dramatically during

Method	BS-ERGB test			HS-ERGB close			HS-ERGB far		
	LPIPS↓	PSNR↑	SSIM↑	LPIPS↓	PSNR↑	SSIM↑	LPIPS↓	PSNR↑	SSIM↑
<i>In-distribution (32 frames)</i>									
HyperE2VID (autoregressive)	0.422	17.2	<u>0.568</u>	0.530	17.7	0.524	0.491	17.0	0.534
LTX-Events (frozen)	<u>0.345</u>	<u>17.8</u>	0.567	<u>0.313</u>	<u>21.1</u>	<u>0.679</u>	<u>0.351</u>	<u>20.1</u>	<u>0.588</u>
LTX-Events (adapted)	0.283	20.3	0.643	0.231	25.4	0.753	0.275	22.8	0.660
<i>Moderate extrapolation (64 frames)</i>									
HyperE2VID (autoregressive)	<u>0.426</u>	16.0	<u>0.549</u>	0.555	15.9	0.465	0.499	15.6	<u>0.515</u>
LTX-Events (frozen)	0.432	<u>16.1</u>	0.488	<u>0.467</u>	<u>17.9</u>	<u>0.551</u>	<u>0.496</u>	<u>17.4</u>	0.501
LTX-Events (adapted)	0.307	19.3	0.609	0.324	21.4	0.651	0.324	21.0	0.602
<i>Extended extrapolation (128 frames)</i>									
HyperE2VID (autoregressive)	0.423	<u>14.8</u>	0.540	0.575	<u>14.4</u>	<u>0.415</u>	0.503	14.6	0.503
LTX-Events (frozen)	0.572	13.4	0.364	0.665	14.2	0.340	0.638	<u>15.1</u>	0.402
LTX-Events (adapted)	0.374	16.8	<u>0.523</u>	0.474	16.6	0.474	0.368	19.0	0.558

Table 1. Architectural comparison and temporal extrapolation. Comparison of our event-conditioned LTX approach against the HyperE2VID autoregressive baseline across three datasets and sequence lengths. “Frozen” (LoRA rank 0) trains only the event encoder; “Adapted” (LoRA rank 32) additionally adapts the LTX transformer. Our adapted approach outperforms HyperE2VID by 33% at 32 frames and achieves strong cross-dataset generalization on HS-ERGB.

extrapolation: at 64 frames, frozen degrades to 0.432 while adapted maintains 0.307 (29% gap); at 128 frames, frozen collapses to 0.572 while adapted reaches 0.374 (35% gap). The frozen model degrades 66% from 32 to 128 frames, while the adapted model degrades only 32%.

This pattern indicates that the event encoder alone is insufficient—the transformer’s attention mechanisms must adapt to integrate event-conditioned features with pre-trained temporal representations.

Temporal extrapolation. Our adapted approach generates sequences up to 4× the training length while maintaining reasonable quality. LPIPS degrades gracefully from 0.283 to 0.374 on BS-ERGB (32% degradation), preserving temporal coherence far beyond the training distribution. In contrast, frozen collapses at longer sequences (66% degradation), and HyperE2VID shows minimal change across lengths (0.422 → 0.423), suggesting it operates near its performance ceiling regardless of sequence length.

Cross-dataset generalization. Despite training exclusively on BS-ERGB, our adapted model achieves strong performance on HS-ERGB: 0.231 LPIPS on close sequences and 0.275 on far sequences—both better than our BS-ERGB test performance (0.283). This demonstrates robust event-to-RGB mapping that transfers across different hardware, frame rates, and scene characteristics. HyperE2VID also generalizes (0.530 and 0.491 LPIPS) but maintains a substantial performance gap.

Figure 3 shows representative generation results comparing our approach against baselines. HyperE2VID fails to maintain background consistency and color stability, with

rapid degradation as sequences progress, reflecting the difficulty of propagating appearance through recurrent architectures without pretrained priors. The frozen LTX variant (event encoder only) shows reasonable early-frame quality but exhibits critical failures in later frames: implausible background hallucinations when moving objects reveal previously occluded regions, and semantic degradation where moving objects dissolve into pixel artifacts rather than maintaining coherent structure.

Our adapted model addresses both issues. Transformer adaptation enables the integration of event-driven motion cues with pretrained scene understanding, maintaining object semantics throughout sequences and generating contextually plausible backgrounds. These qualitative differences explain the 18% performance gap between frozen and adapted variants in Table 1 (0.345 vs. 0.283 LPIPS).

4.2.1. Injection Point Ablation

Injection Strategy	LPIPS↓	PSNR↑	SSIM↑
Layer 1 only (first)	0.309	18.4	0.591
Layer 14 only (middle)	<u>0.305</u>	18.8	<u>0.597</u>
Layer 28 only (last)	0.318	<u>19.1</u>	0.586
LTX-Events (all layers)	0.283	20.3	0.643
HyperE2VID	0.422	17.2	0.568

Table 2. LTX Event injection point ablation. Dense injection outperforms single-layer injection, with all variants substantially improving over HyperE2VID. Evaluated on BS-ERGB test, 32 frames.

To understand where event conditioning is most critical in the transformer hierarchy, we ablate the injection strategy (Table 2). Injecting events at a single layer—whether early (layer 1: 0.309 LPIPS), middle (layer 14: 0.305), or late (layer 28: 0.318)—yields 9–12% worse performance than dense injection at all 28 layers (0.283 LPIPS). However, even single-layer injection substantially outperforms the autoregressive baseline (0.422 LPIPS, 27–37% improvement), demonstrating the robustness of our event conditioning approach regardless of injection configuration.

The relatively similar performance across single-layer locations (0.305–0.318 range) suggests that no individual transformer layer is uniquely critical for event integration. Dense injection achieves optimal performance by enabling cumulative integration of event information throughout the transformer hierarchy, allowing each block to modulate its spatiotemporal reasoning based on event-driven motion cues.

4.2.2. Event Representation Ablation

Event streams can be represented through different design choices: temporal binning granularity (how many bins to accumulate events into per frame interval) and polarity encoding (how to handle positive and negative brightness changes). For our experiments, we used 5-bin difference encoding to maintain consistency with prior event-based work [4]. Here, we systematically evaluate whether the choice of event representation impacts reconstruction quality.

Polarity Encoding	N_{bins}	LPIPS \downarrow	PSNR \uparrow	SSIM \uparrow
Difference	1	0.282	20.3	0.646
Difference (default)	5	0.283	20.3	0.643
Difference	10	0.285	20.4	0.648
Concatenation	5	0.281	20.5	0.648

Table 3. **Event representation ablation.** All representations achieve comparable performance, demonstrating robustness to temporal binning and polarity encoding choices. Evaluated on BS-ERGB test, 32 frames.

Table 3 shows that all representations achieve comparable performance, with LPIPS scores ranging from 0.281 to 0.285 (within 1.4%). Temporal binning has minimal impact: using a single bin (0.282 LPIPS)—which collapses all events in the frame interval into one accumulation—performs nearly identically to 10 bins (0.285 LPIPS). Similarly, polarity encoding choice (difference vs. concatenation) yields negligible differences (0.283 vs. 0.281 LPIPS).

These findings demonstrate that our approach is robust to event representation choices. In practice, this means simpler representations (e.g., single bin) can be used without sacrificing quality.

4.2.3. Conditioning Strategy

Event-based frame interpolation methods condition on both first and last frames alongside the intervening event stream [3]. This bidirectional conditioning is effective for interpolation scenarios with small motion and short temporal spans (typically 1–3 intermediate frames). We evaluate whether this strategy benefits our reconstruction task, which generates longer sequences (32+ frames) with potentially large cumulative motion from a single initial frame.

Conditioning	LPIPS \downarrow	PSNR \uparrow	SSIM \uparrow
Unidirectional (first only)	0.283	20.3	0.643
Bidirectional (first + last)	0.283	20.5	0.651

Table 4. **Frame Conditioning strategy ablation.** Evaluated on BS-ERGB test, 32 frames.

Table 4 shows that bidirectional conditioning (first + last frame) provides virtually no performance improvement over unidirectional conditioning (first frame only): both achieve 0.283 LPIPS at 32 frames. This suggests that for long-range reconstruction with large motion, the additional constraint from the endpoint frame does not improve intermediate frame generation. The event stream provides sufficient motion information to guide generation without requiring the target endpoint.

For simplicity and practical deployment scenarios where capturing the last frame may not be feasible, we use unidirectional conditioning for all experiments.

5. Conclusion

We introduced RGB video generation from sparse keyframes and event camera data, demonstrating a practical paradigm for power-efficient video capture: record minimal RGB frames alongside continuous event streams, then reconstruct full RGB video offline where computational resources are abundant. This hybrid approach addresses a fundamental bottleneck in battery-operated vision systems—continuous RGB capture is power-prohibitive, yet many applications require standard video output rather than raw event data. Through systematic experiments, we demonstrated that adapting pretrained video diffusion models through event injection achieves 33% better perceptual quality than autoregressive baselines while maintaining strong cross-dataset generalization. Our approach generates sequences up to 4 \times training length, validating extreme temporal extrapolation from sparse RGB observations when guided by dense event data. These results establish event-conditioned video generation as a viable approach for power-constrained video capture systems, opening new possibilities for long-duration surveillance, mobile robotics, and wearable vision applications.

Acknowledgments

This work presented in this paper was funded by the U.S. Department of Energy (DOE), National Nuclear Security Administration, Office of Defense Nuclear Nonproliferation Research and Development. The manuscript has been authored by Brookhaven National Laboratory managed by Brookhaven Science Associates, LLC under the Contract No. DE-SC0012704 with the U.S. Department of Energy.

Yonggang Cui is currently affiliated with the IAEA (International Atomic Energy Agency). His contributions to this paper were completed entirely during his prior employment period at Brookhaven National Laboratory (BNL). Therefore, this work does not reflect any contribution or endorsement by the IAEA, nor does his current affiliation imply any conflict of interest regarding the presented research.

References

- [1] Andreas Blattmann, Tim Dockhorn, Sumith Kulal, Daniel Mendelevitch, Maciej Kilian, Dominik Lorenz, Yam Levi, Zion English, Vikram Voleti, Adam Letts, Varun Jampani, and Robin Rombach. Stable video diffusion: Scaling latent video diffusion models to large datasets, 2023. [3](#), [4](#)
- [2] Junsong Chen, Jincheng Yu, Chongjian Ge, Lewei Yao, Enze Xie, Yue Wu, Zhongdao Wang, James Kwok, Ping Luo, Huchuan Lu, et al. Pixart: Fast training of diffusion transformer for photorealistic text-to-image synthesis. *arXiv preprint arXiv:2310.00426*, 2023. [4](#)
- [3] Jingxi Chen, Brandon Y. Feng, Haoming Cai, Tianfu Wang, Levi Burner, Dehao Yuan, Cornelia Fermuller, Christopher A. Metzler, and Yiannis Aloimonos. Repurposing pre-trained video diffusion models for event-based video interpolation, 2025. [2](#), [4](#), [8](#)
- [4] Burak Ercan, Onur Eker, Canberk Saglam, Aykut Erdem, and Erkut Erdem. Hypere2vid: Improving event-based video reconstruction via hypernetworks. *IEEE Transactions on Image Processing*, 33:1826–1837, 2024. [2](#), [3](#), [6](#), [8](#), [11](#)
- [5] Guillermo Gallego, Tobi Delbruck, Garrick Orchard, Chiara Bartolozzi, Brian Taba, Andrea Censi, Stefan Leutenegger, Andrew J. Davison, Jorg Conradt, Kostas Daniilidis, and Davide Scaramuzza. Event-based vision: A survey. *IEEE Transactions on Pattern Analysis and Machine Intelligence*, 44(1):154–180, 2022. [1](#), [2](#)
- [6] David Ha, Andrew M. Dai, and Quoc V. Le. Hypernetworks. In *5th International Conference on Learning Representations, ICLR 2017, Toulon, France, April 24-26, 2017, Conference Track Proceedings*. OpenReview.net, 2017. [2](#), [3](#), [11](#)
- [7] Yoav HaCohen, Nisan Chiprut, Benny Brazowski, Daniel Shalem, Dudu Moshe, Eitan Richardson, Eran Levin, Guy Shiran, Nir Zabari, Ori Gordon, Poriya Panet, Sapir Weissbuch, Victor Kulikov, Yaki Bitterman, Zeev Melumian, and Ofir Bibi. Ltx-video: Realtime video latent diffusion, 2024. [2](#), [3](#), [4](#), [10](#)
- [8] Weihua He, Kaichao You, Zhendong Qiao, Xu Jia, Ziyang Zhang, Wenhui Wang, Huchuan Lu, Yaoyuan Wang, and Jianxing Liao. Timereplayer: Unlocking the potential of event cameras for video interpolation, 2022. [2](#)
- [9] D Hendrycks. Gaussian error linear units (gelus). *arXiv preprint arXiv:1606.08415*, 2016. [10](#)
- [10] Jonathan Ho, Ajay Jain, and Pieter Abbeel. Denoising diffusion probabilistic models. In *Advances in Neural Information Processing Systems 33: Annual Conference on Neural Information Processing Systems 2020, NeurIPS 2020, December 6-12, 2020, virtual*, 2020. [2](#)
- [11] Edward J Hu, Yelong Shen, Phillip Wallis, Zeyuan Allen-Zhu, Yuanzhi Li, Shean Wang, Lu Wang, Weizhu Chen, et al. Lora: Low-rank adaptation of large language models. *ICLR*, 1(2):3, 2022. [3](#), [5](#), [10](#)
- [12] Kinam Kim, Junha Hyung, and Jaegul Choo. Temporal in-context fine-tuning for versatile control of video diffusion models. *CorR*, abs/2506.00996, 2025. [3](#)
- [13] Xingchao Liu, Chengyue Gong, and Qiang Liu. Flow straight and fast: Learning to generate and transfer data with rectified flow. In *The Eleventh International Conference on Learning Representations, ICLR 2023, Kigali, Rwanda, May 1-5, 2023*. OpenReview.net, 2023. [4](#), [5](#)
- [14] Yue Ma, Kunyu Feng, Zhongyuan Hu, Xinyu Wang, Yucheng Wang, Mingzhe Zheng, Xuanhua He, Chenyang Zhu, Hongyu Liu, Yingqing He, Zeyu Wang, Zhifeng Li, Xiu Li, Wei Liu, Dan Xu, Linfeng Zhang, and Qifeng Chen. Controllable video generation: A survey, 2025. [3](#)
- [15] William Peebles and Saining Xie. Scalable diffusion models with transformers. In *IEEE/CVF International Conference on Computer Vision, ICCV 2023, Paris, France, October 1-6, 2023*, pages 4172–4182. IEEE, 2023. [4](#)
- [16] Adam Polyak, Amit Zohar, Andrew Brown, Andros Tjandra, Animesh Sinha, Ann Lee, Apoorv Vyas, Bowen Shi, Chih-Yao Ma, Ching-Yao Chuang, et al. Movie gen: A cast of media foundation models. *arXiv preprint arXiv:2410.13720*, 2024. [4](#)
- [17] Henri Rebecq, René Ranftl, Vladlen Koltun, and Davide Scaramuzza. High speed and high dynamic range video with an event camera. *IEEE Trans. Pattern Anal. Mach. Intell.*, 43(6):1964–1980, 2021. [2](#), [3](#)
- [18] Robin Rombach, Andreas Blattmann, Dominik Lorenz, Patrick Esser, and Björn Ommer. High-resolution image synthesis with latent diffusion models, 2022. [2](#)
- [19] Olaf Ronneberger, Philipp Fischer, and Thomas Brox. U-net: Convolutional networks for biomedical image segmentation. In *International Conference on Medical image computing and computer-assisted intervention*, pages 234–241. Springer, 2015. [4](#)
- [20] Cedric Scheerlinck, Henri Rebecq, Daniel Gehrig, Nick Barnes, Robert E. Mahony, and Davide Scaramuzza. Fast image reconstruction with an event camera. In *IEEE Winter Conference on Applications of Computer Vision, WACV 2020, Snowmass Village, CO, USA, March 1-5, 2020*, pages 156–163. IEEE, 2020. [2](#)
- [21] Xingjian Shi, Zhourong Chen, Hao Wang, Dit-Yan Yeung, Wai-Kin Wong, and Wang-chun Woo. Convolutional LSTM network: A machine learning approach for precipitation nowcasting. In *Advances in Neural Information Processing Systems 28: Annual Conference on Neural Information Processing Systems*

Processing Systems 2015, December 7-12, 2015, Montreal, Quebec, Canada, pages 802–810, 2015. 2, 3, 11

[22] Gurkirt Singh and Fabio Cuzzolin. Recurrent convolutions for causal 3d cnns. In *Proceedings of the IEEE/CVF International Conference on Computer Vision Workshops*, pages 0–0, 2019. 5

[23] Timo Stoffregen, Cedric Scheerlinck, Davide Scaramuzza, Tom Drummond, Nick Barnes, Lindsay Kleeman, and Robert E. Mahony. Reducing the sim-to-real gap for event cameras. In *Computer Vision - ECCV 2020 - 16th European Conference, Glasgow, UK, August 23-28, 2020, Proceedings, Part XXVII*, pages 534–549. Springer, 2020. 2

[24] Zachary Teed and Jia Deng. RAFT: recurrent all-pairs field transforms for optical flow. In *Computer Vision - ECCV 2020 - 16th European Conference, Glasgow, UK, August 23-28, 2020, Proceedings, Part II*, pages 402–419. Springer, 2020. 11

[25] Stepan Tulyakov, Daniel Gehrig, Stamatios Georgoulis, Julius Erbach, Mathias Gehrig, Yuanyou Li, and Davide Scaramuzza. Timelens: Event-based video frame interpolation, 2021. 2, 5, 11

[26] Stepan Tulyakov, Alfredo Bochicchio, Daniel Gehrig, Stamatios Georgoulis, Yuanyou Li, and Davide Scaramuzza. Time lens++: Event-based frame interpolation with parametric non-linear flow and multi-scale fusion, 2022. 2, 5, 10, 11

[27] Xiang Wang, Hangjie Yuan, Shiwei Zhang, Dayou Chen, Jiniu Wang, Yingya Zhang, Yujun Shen, Deli Zhao, and Jingen Zhou. Videocomposer: Compositional video synthesis with motion controllability. In *Advances in Neural Information Processing Systems 36: Annual Conference on Neural Information Processing Systems 2023, NeurIPS 2023, New Orleans, LA, USA, December 10 - 16, 2023*, 2023. 2, 3

[28] Ziyun Wang, Friedhelm Hamann, Kenneth Chaney, Wen Jiang, Guillermo Gallego, and Kostas Daniilidis. Event-based continuous color video decompression from single frames. In *IEEE/CVF Conference on Computer Vision and Pattern Recognition Workshops, CVPR Workshops 2025, Nashville, TN, USA, June 11-15, 2025*, pages 4968–4978. Computer Vision Foundation / IEEE, 2025. 2

[29] Wenming Weng, Yueyi Zhang, and Zhiwei Xiong. Event-based video reconstruction using transformer. In *2021 IEEE/CVF International Conference on Computer Vision, ICCV 2021, Montreal, QC, Canada, October 10-17, 2021*, pages 2543–2552. IEEE, 2021. 2

[30] Ronald J Williams and Jing Peng. An efficient gradient-based algorithm for on-line training of recurrent network trajectories. *Neural computation*, 2(4):490–501, 1990. 3

[31] Jay Zhangjie Wu, Yixiao Ge, Xintao Wang, Stan Weixian Lei, Yuchao Gu, Yufei Shi, Wynne Hsu, Ying Shan, Xiaohu Qie, and Mike Zheng Shou. Tune-a-video: One-shot tuning of image diffusion models for text-to-video generation. In *IEEE/CVF International Conference on Computer Vision, ICCV 2023, Paris, France, October 1-6, 2023*, pages 7589–7599. IEEE, 2023. 2, 3

[32] Zhuoyi Yang, Jiayan Teng, Wendi Zheng, Ming Ding, Shiyu Huang, Jiazheng Xu, Yuanming Yang, Wenyi Hong, Xiaohan Zhang, Guanyu Feng, Da Yin, Yuxuan Zhang, Weihan Wang, Yean Cheng, Bin Xu, Xiaotao Gu, Yuxiao Dong, and Jie Tang. Cogvideox: Text-to-video diffusion models with an expert transformer. In *The Thirteenth International Conference on Learning Representations, ICLR 2025, Singapore, April 24-28, 2025*. OpenReview.net, 2025. 4

[33] Biao Zhang and Rico Sennrich. Root mean square layer normalization. In *Advances in Neural Information Processing Systems 32: Annual Conference on Neural Information Processing Systems 2019, NeurIPS 2019, December 8-14, 2019, Vancouver, BC, Canada*, pages 12360–12371, 2019. 10

[34] Lvmin Zhang, Anyi Rao, and Maneesh Agrawala. Adding conditional control to text-to-image diffusion models, 2023. 3, 4, 5

[35] Richard Zhang, Phillip Isola, Alexei A Efros, Eli Shechtman, and Oliver Wang. The unreasonable effectiveness of deep features as a perceptual metric. In *Proceedings of the IEEE conference on computer vision and pattern recognition*, pages 586–595, 2018. 3, 6, 11

6. Implementation Details

6.1. LTX Model Training

We train our event-conditioned LTX model on the BSERGB dataset [26] using the following configuration.

Model Architecture. We use the pretrained LTX-Video model from Lightricks [7] with Low-Rank Adaptation (LoRA) applied to the transformer’s attention and feed-forward layers [11]. The base transformer contains 28 layers with 32 attention heads, attention head dimension 64, and hidden dimension 2048 (32×64). We use LoRA rank 32 by default, adding approximately 48.8M trainable parameters while keeping the 1.9B pretrained weights frozen.

Our event encoder follows an FPN-style architecture mimicking the VAE encoder of the LTX model with the following structure:

- **Stem block:** 128 channels with spatial patch size 4 and temporal patch size 1
- **Downsampling blocks:** Progressive channel expansion ($128 \rightarrow 256 \rightarrow 512 \rightarrow 512$) with spatiotemporal scaling applied to the first three blocks
- **Mid-level blocks:** 28 processing blocks (one per transformer layer), each with 1 residual layer, outputting 2048-channel features via learned projections
- **Architectural details:** RMSNorm [33] with $\epsilon = 10^{-6}$, causal 3D convolutions, GELU activation [9]

The event encoder processes 5-bin stacked histogram representations with difference encoding (positive minus negative polarity), yielding input tensors of shape (5, 256, 256).

Training Configuration. We train for 400 epochs with batch size 4 on video clips of 32 frames at 256×256 resolution. We use the AdamW optimizer with learning rate 10^{-5} and no weight decay. Training data augmentation includes random horizontal flips and random resized crops with scale

range $[0.2, 1.0]$. Each training epoch consists of 250 gradient steps. Video clips are sampled with stride 1 and drop incomplete sequences to ensure all clips contain exactly 32 frames.

Compute Resources. All models train on NVIDIA A6000 GPUs (48GB VRAM) with mixed precision (bfloat16). Training time is approximately 75 hours per 400-epoch run on a single GPU.

6.2. HyperE2VID Baseline Training

We train our adapted HyperE2VID baseline on the BS-ERGB dataset [26] using the following configuration.

Model Architecture. We adapt the HyperE2VID architecture [4] for RGB video generation conditioned on an initial frame. The model uses a U-Net encoder-decoder structure with ConvLSTM recurrent blocks [21] and dynamic convolutions generated via hypernetworks [6]. The architecture consists of:

- **Encoder:** 3 downsampling stages with base channel count 32 and channel multiplier 2, yielding channel progression $(32 \rightarrow 64 \rightarrow 128)$
- **Recurrent blocks:** ConvLSTM with kernel size 5 at each encoder level
- **Decoder:** Symmetric upsampling path with sum-based skip connections, 2 residual blocks per level, and dynamic decoder enabled
- **Context fusion:** Processes 5-bin event histograms alongside 3-channel previous RGB reconstruction
- **Output:** 3-channel RGB frames (modified from original single-channel intensity output)

The model processes 5-bin stacked histogram representations with difference encoding, matching the event representation used for the diffusion approach.

Training Configuration. We train for 400 epochs with batch size 10 on video sequences of 40 frames at 256×256 resolution. We use the AdamW optimizer with learning rate 10^{-4} (lower than the 10^{-3} used in the original HyperE2VID paper, which we found to improve stability and final performance) and no weight decay.

Following the original HyperE2VID training strategy, we employ Truncated Backpropagation Through Time (TBPTT) with truncation period 5 timesteps, computing losses every 10 timesteps. We use curriculum learning with teacher forcing linearly annealed over the first 100 epochs (25% of training): during this period, the input previous frame is a weighted combination $\beta \cdot \hat{\mathbf{I}}_{t-1} + (1 - \beta) \cdot \mathbf{I}_{t-1}$ where β increases from 0 to 1. After epoch 100, the model trains in fully autoregressive mode.

The loss combines perceptual quality and temporal consistency: $\mathcal{L}_{\text{total}} = \mathcal{L}_{\text{LPIPS}} + \mathcal{L}_{\text{flow}}$ where $\mathcal{L}_{\text{LPIPS}}$ is the learned perceptual loss [35] with AlexNet backbone, and $\mathcal{L}_{\text{flow}}$ is the optical flow consistency loss. Since BS-ERGB does not

provide optical flow annotations, we compute optical flow on-the-fly during training using the RAFT model [24].

Training data augmentation includes random horizontal flips, random vertical flips, and random resized crops with scale range $[0.2, 1.0]$.

Compute Resources. Training uses NVIDIA A6000 GPUs with full precision (float32). Training time is approximately 87 hours per 400-epoch run on a single GPU.

6.3. Evaluation Protocol

We evaluate all models (diffusion-based and autoregressive) using a consistent protocol to ensure fair comparison. Test sequences are preprocessed deterministically: frames are resized via bilinear interpolation such that the shorter side equals 256 pixels while preserving aspect ratio, then center-cropped to 256×256 . Event histograms undergo identical spatial transformations to maintain alignment with RGB frames.

Evaluation Sampling. We sample clips from test videos with stride 16 frames: for a video of length T , we extract clips starting at frames $\{0, 16, 32, \dots\}$ until fewer than the target clip length remains. This provides multiple evaluation examples per video while maintaining temporal diversity.

Sequence Generation. The diffusion model generates sequences of arbitrary length (32, 64, or 128 frames) in a single forward pass using 50 rectified flow steps. The autoregressive baseline generates frames sequentially through its recurrent architecture.

Metrics. We compute LPIPS [35] with AlexNet backbone, PSNR, and SSIM on all generated frames at 256×256 resolution. Metrics are averaged across all frames in each sequence, then averaged across all sequences in the test set.

Test Sets. We evaluate on three datasets: BS-ERGB [26] test split (same domain as training), HS-ERGB [25] close setting (9 sequences, ~ 11 k frames), and HS-ERGB far setting (6 sequences, ~ 5 k frames).

7. Qualitative Results

7.1. Cross-Dataset Generalization (32 frames)

Figure 4–6 show representative qualitative results at the training sequence length (32 frames) across all three evaluation datasets. These examples establish baseline reconstruction quality before examining temporal extrapolation and failure modes in subsequent sections.

Our adapted method consistently maintains temporal coherence and photometric accuracy across diverse motion patterns and capture conditions. Figure 4 demonstrates in-distribution reconstruction of complex human motion on BS-ERGB. Figure 5 shows successful handling of fast non-linear dynamics (water balloon burst) on HS-ERGB close,

despite differences in capture hardware and scene characteristics from the training distribution. Figure 6 illustrates robust performance under egocentric camera motion at long range on HS-ERGB far, where the model must plausibly hallucinate newly visible regions as the viewpoint changes.

In contrast, the HyperE2VID baseline exhibits progressive background inconsistencies and color drift across all datasets, reflecting the difficulty of maintaining appearance through autoregressive propagation without pretrained temporal priors. The Frozen LTX variant (event encoder only, no transformer adaptation) produces plausible early frames but shows reduced temporal consistency compared to our fully adapted approach, particularly visible in later frames where accumulated errors become apparent.

7.2. Limitations and Failure Modes

While our method achieves strong performance under typical conditions, we identify three primary failure modes that represent current limitations.

Motion blur on fast objects. Figure 7 shows motion blur artifacts on a rapidly spinning basketball captured at 28 FPS. The model produces blur consistent with natural camera exposure at standard frame rates, reflecting priors inherited from LTX’s pretraining on conventional video datasets. However, since event cameras provide microsecond temporal resolution, fast motion can be handled by rebinning events at higher target frame rates during reconstruction—our successful results on HS-ERGB (150+ FPS, Figure 5) demonstrate that the model adapts to higher temporal sampling when event data is rebinned accordingly.

Fine texture degradation. Figure 8 demonstrates progressive loss of fine pattern details on a rotating umbrella with intricate texture. Complex high-frequency umbrella pattern blurs into coarser regions as the sequence advances, reflecting the diffusion model’s tendency to prioritize structural coherence over fine texture preservation under motion. Despite this local texture degradation, overall scene semantics and temporal consistency remain intact.

Extreme extrapolation breakdown. Figure 9 illustrates catastrophic failure when extrapolating far beyond the training distribution. At $4\times$ the training sequence length (128 frames) on out-of-domain data (HS-ERGB close), the stationary person progressively fades after frame ~ 32 (the training length boundary) and the model hallucinates implausible background content. This breakdown occurs specifically under the combination of extreme temporal extrapolation and cross-dataset evaluation; in-distribution results on BS-ERGB maintain consistency even at 128 frames (see Section 7.3).

7.3. Temporal Extrapolation

We evaluate temporal extrapolation beyond the training sequence length by generating videos of 64 frames ($2\times$ training length) and 128 frames ($4\times$ training length). Figures 10–15 show representative results across all three datasets at both extrapolation horizons.

Our adapted method maintains reasonable quality and temporal coherence even at $4\times$ the training length. While perceptual quality degrades gracefully with sequence length (Table 1 in main paper: $0.283 \rightarrow 0.307 \rightarrow 0.374$ LPIPS at 32/64/128 frames on BS-ERGB), the model preserves structural plausibility and scene semantics throughout extended sequences. Figures 10 and 13 demonstrate consistent in-distribution extrapolation on BS-ERGB, with complex motion patterns (horse locomotion, juggling) remaining coherent across the full temporal span. Cross-dataset extrapolation (Figures 11–15) shows similarly robust behavior on HS-ERGB, maintaining quality despite differences in capture hardware and scene characteristics.

In contrast, the Frozen LTX baseline exhibits significant quality degradation at long horizons. Without transformer adaptation, accumulated artifacts and temporal inconsistencies compound beyond the training length, with later frames showing reduced coherence and increasing perceptual artifacts. The HyperE2VID baseline exhibits poor quality across all sequence lengths ($0.422 \rightarrow 0.423$ LPIPS on BS-ERGB), with minimal variation indicating that its autoregressive errors saturate immediately rather than accumulating with large temporal spans.

These results demonstrate that transformer adaptation via LoRA is critical not only for baseline quality but specifically for stable temporal extrapolation, enabling the model to maintain coherence far beyond its training distribution while both the frozen variant and autoregressive baseline fail under the same conditions.

8. Additional Ablations

8.0.1. Transformer Adaptation Capacity

Model	LoRA Rank	LPIPS \downarrow	PSNR \uparrow	SSIM \uparrow
LTX-Events	0 (frozen)	0.345	17.8	0.567
LTX-Events	8	0.286	20.1	0.639
LTX-Events	32 (default)	0.283	20.3	0.643
LTX-Events	128	0.286	20.2	0.640

Table 5. **LoRA rank ablation.** Transformer adaptation is essential (rank 0 fails), but minimal capacity (rank 8) is sufficient with diminishing returns beyond. Evaluated on BS-ERGB test, 32 frames.

Our approach adapts the pretrained LTX transformer using Low-Rank Adaptation (LoRA) while keeping the base weights frozen. To understand the necessary adaptation ca-

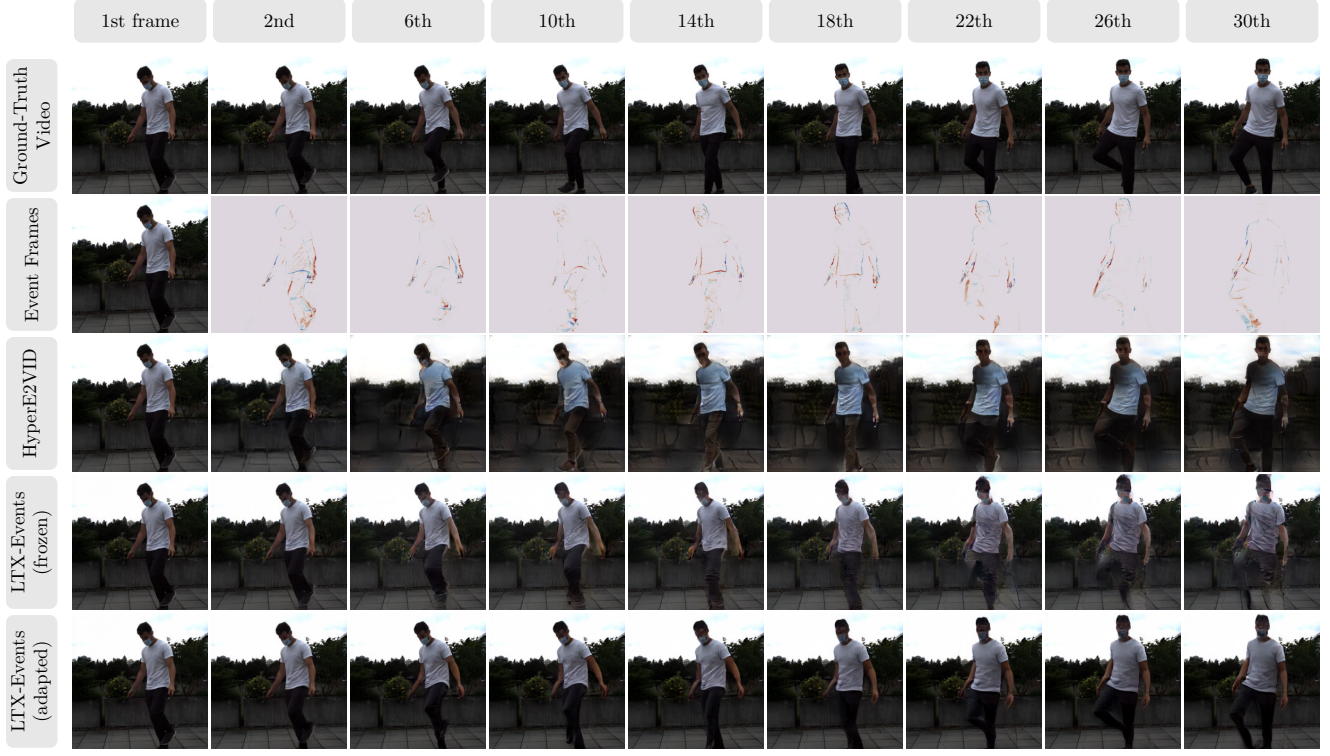


Figure 4. Qualitative comparison on BS-ERGB (32 frames) showing a person preparing to jump. Column labels indicate frame numbers.



Figure 5. Qualitative comparison on HS-ERGB close (32 frames) showing a water balloon falling and bursting. Column labels indicate frame numbers.



Figure 6. Qualitative comparison on HS-ERGB far (32 frames) showing egocentric camera motion in a far-field outdoor scene. Column labels indicate frame numbers.

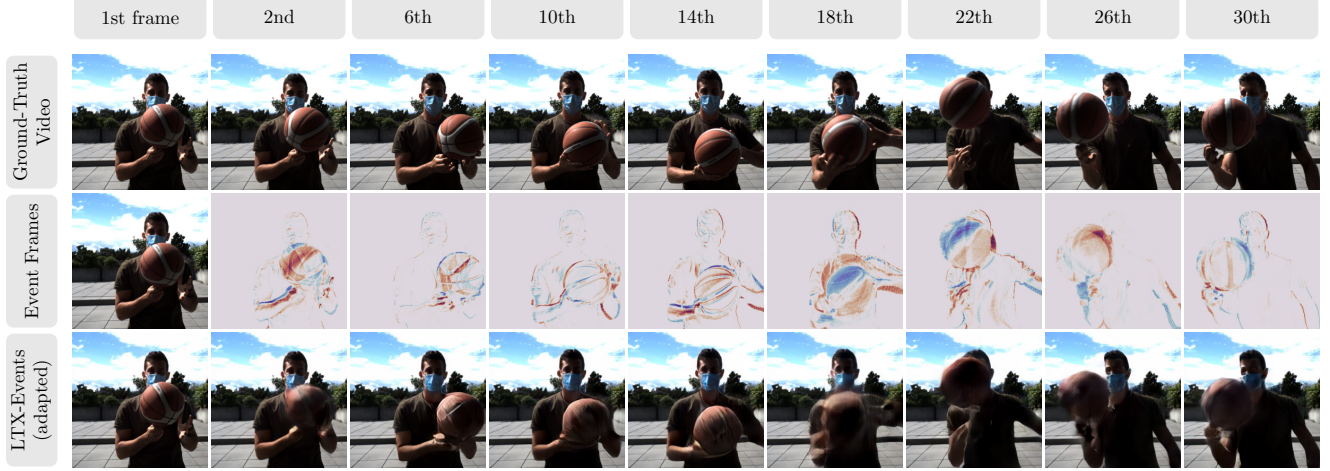


Figure 7. Motion blur on fast-moving objects. BS-ERGB (32 frames) showing a person spinning a basketball. The rapidly rotating ball exhibits motion blur consistent with standard video capture. Column labels indicate frame numbers.

capacity, we ablate the LoRA rank from 0 (no adaptation, event encoder only) to 128.

Table 5 reveals two key findings. First, transformer adaptation provides substantial improvement: without LoRA (rank 0), performance degrades to 0.345 LPIPS—still better than the autoregressive baseline (0.422) but 18% worse than adapted variants. This confirms our earlier observation from the main paper that while the event encoder alone

enables better-than-baseline generation, transformer adaptation is necessary to achieve optimal performance by learning to integrate event-conditioned features with pretrained temporal representations.

Second, minimal adaptation capacity is sufficient: rank 8 achieves 0.286 LPIPS, nearly matching rank 32 (0.283) and rank 128 (0.286). The performance plateau beyond rank 8 demonstrates diminishing returns from increased capac-

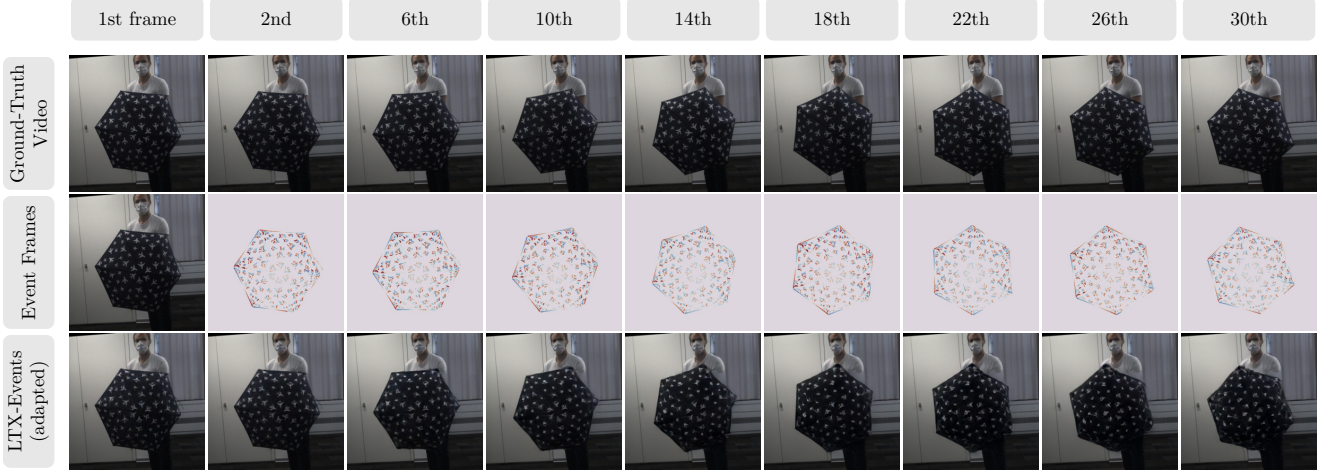


Figure 8. Detail loss on complex patterns. HS-ERGB close (32 frames) showing an umbrella with intricate texture being rotated. Fine pattern details progressively blur as the sequence advances. Column labels indicate frame numbers.

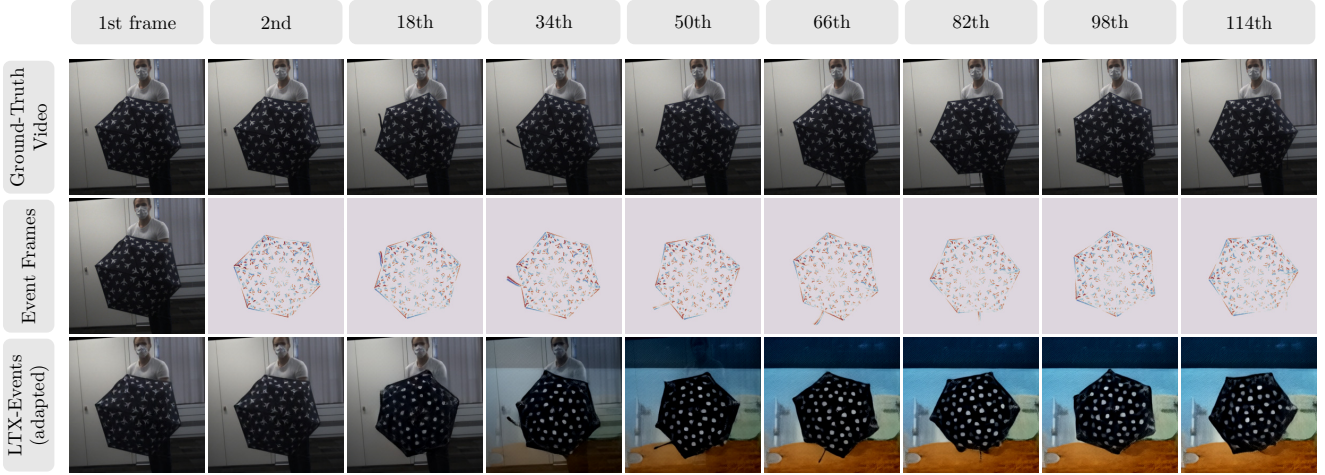


Figure 9. Long-range extrapolation failure on out-of-domain data. HS-ERGB close (128 frames, 4× training length). The stationary person disappears after frame 32 as the model hallucinates an incorrect background, demonstrating a breakdown when extrapolating far beyond the training distribution on cross-dataset evaluation. Column labels indicate frame numbers.

ity. For our experiments, we use rank 32 as a conservative default, though rank 8 would be sufficient for applications requiring maximum parameter efficiency.

9. Resolution Extrapolation

We evaluate whether our model trained at 256×256 resolution can generate higher-resolution outputs by directly inferring at 512×512 (2× spatial upscaling). Table 6 shows results on BS-ERGB at 32 frames.

The model successfully generates 512×512 videos without retraining, though perceptual quality degrades moderately (LPIPS: $0.283 \rightarrow 0.320$, 13% increase). SSIM improves at higher resolution ($0.643 \rightarrow 0.756$), indicating preserved structural coherence, though the LPIPS increase suggests subtle perceptual artifacts emerge when extrapolating beyond the training resolution. This demonstrates practical applicability for 2× resolution deployment without retraining, though optimal quality at higher resolutions would require training at the target resolution.

Model	Resolution	LPIPS↓	PSNR↑	SSIM↑
LTX-Events	256 (default)	0.283	20.3	0.643
LTX-Events	512	0.320	20.8	0.756

Table 6. Resolution extrapolation. Model trained at 256×256 evaluated at native and 2× resolution on BS-ERGB (32 frames).



Figure 10. Qualitative comparison on BS-ERGB (64 frames) showing a horse in motion. Column labels indicate frame numbers.

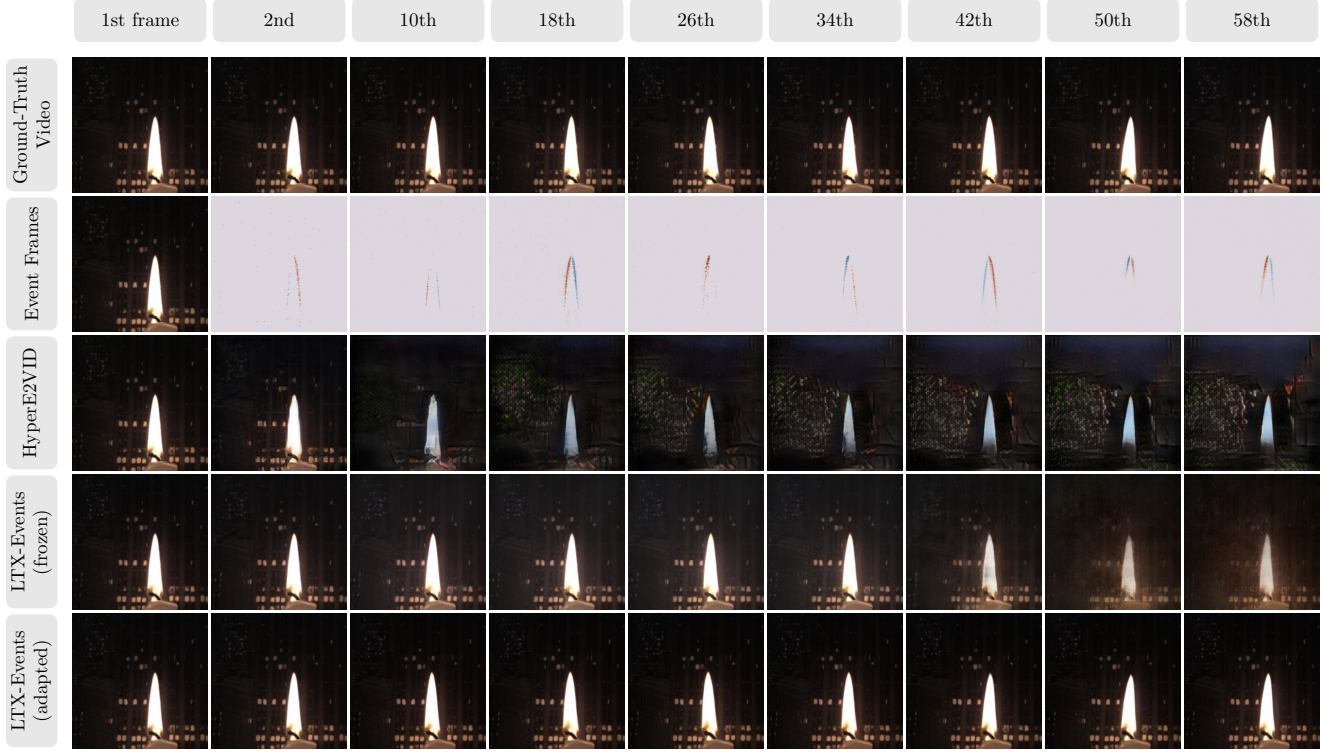


Figure 11. Qualitative comparison on HS-ERGB close (64 frames) showing a flickering candle flame. Column labels indicate frame numbers.

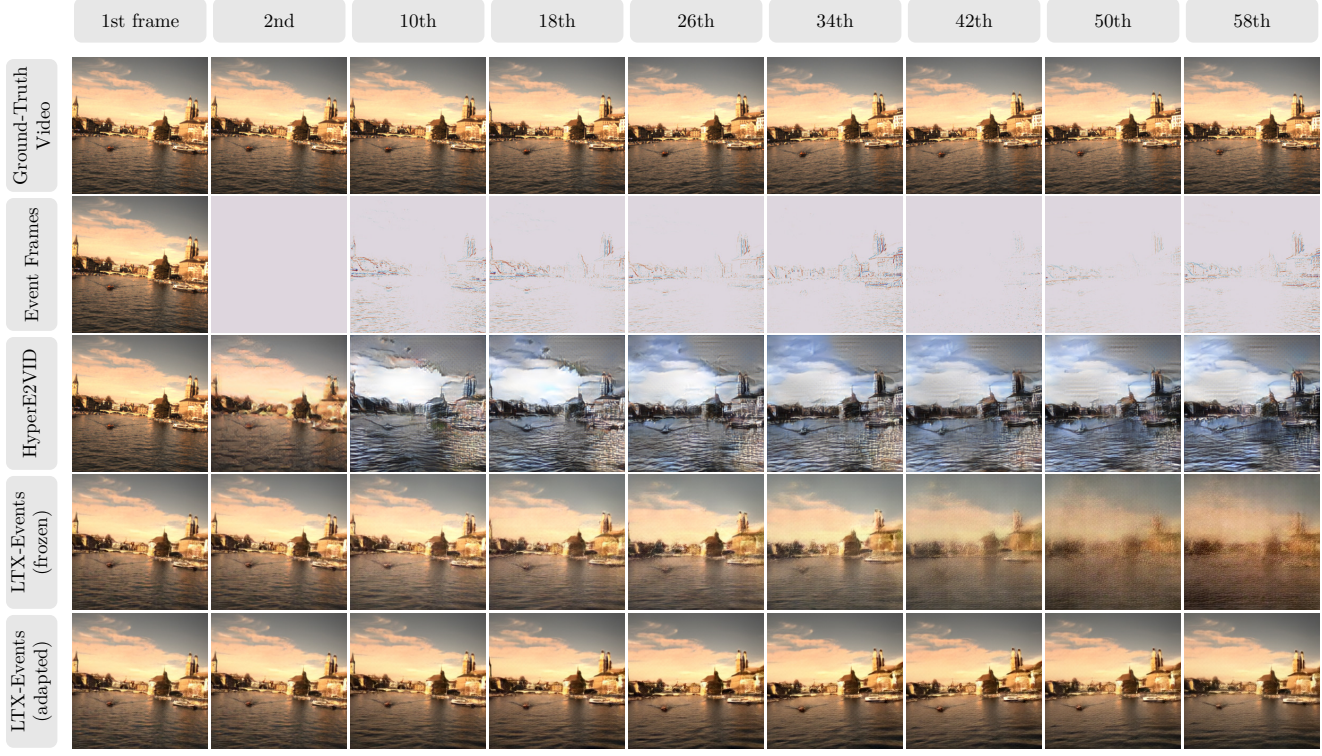


Figure 12. Qualitative comparison on HS-ERGB far (64 frames) showing egocentric camera motion in a far-field outdoor scene. Column labels indicate frame numbers.

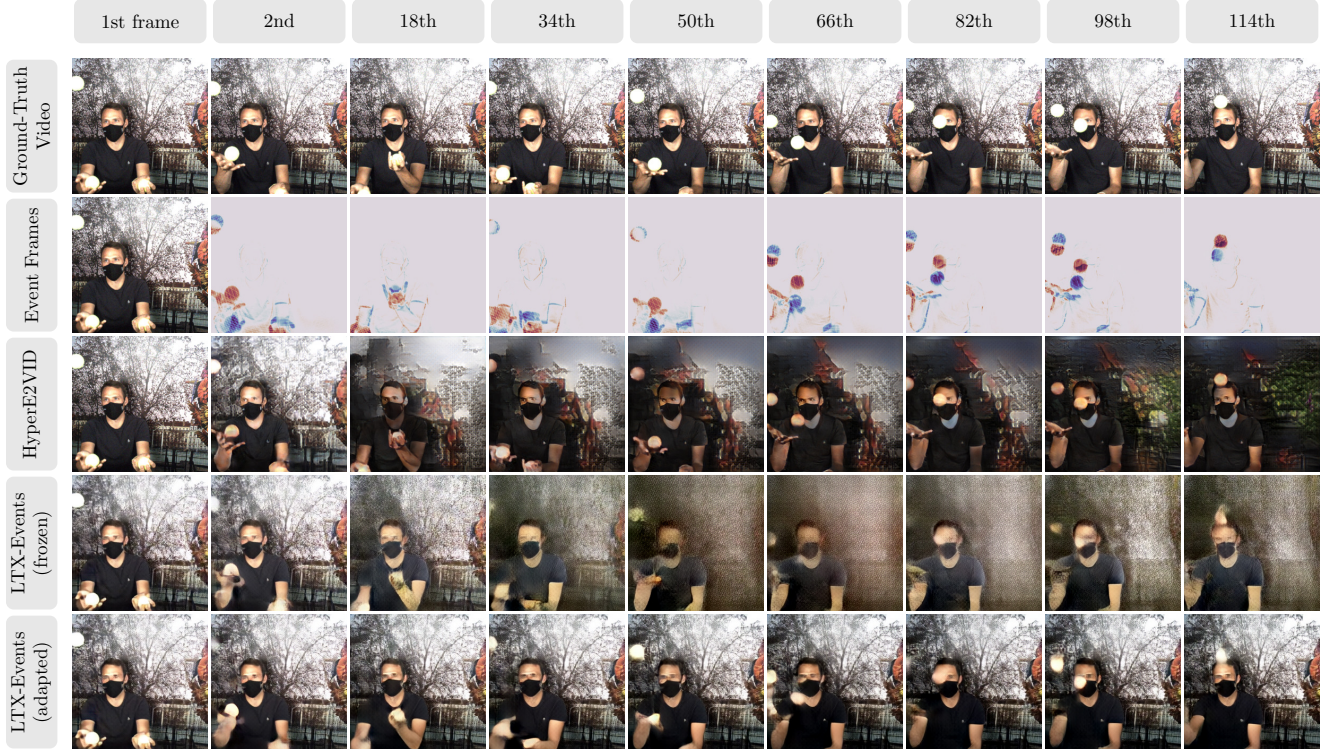


Figure 13. Qualitative comparison on BS-ERGB (128 frames) showing a person juggling. Column labels indicate frame numbers.

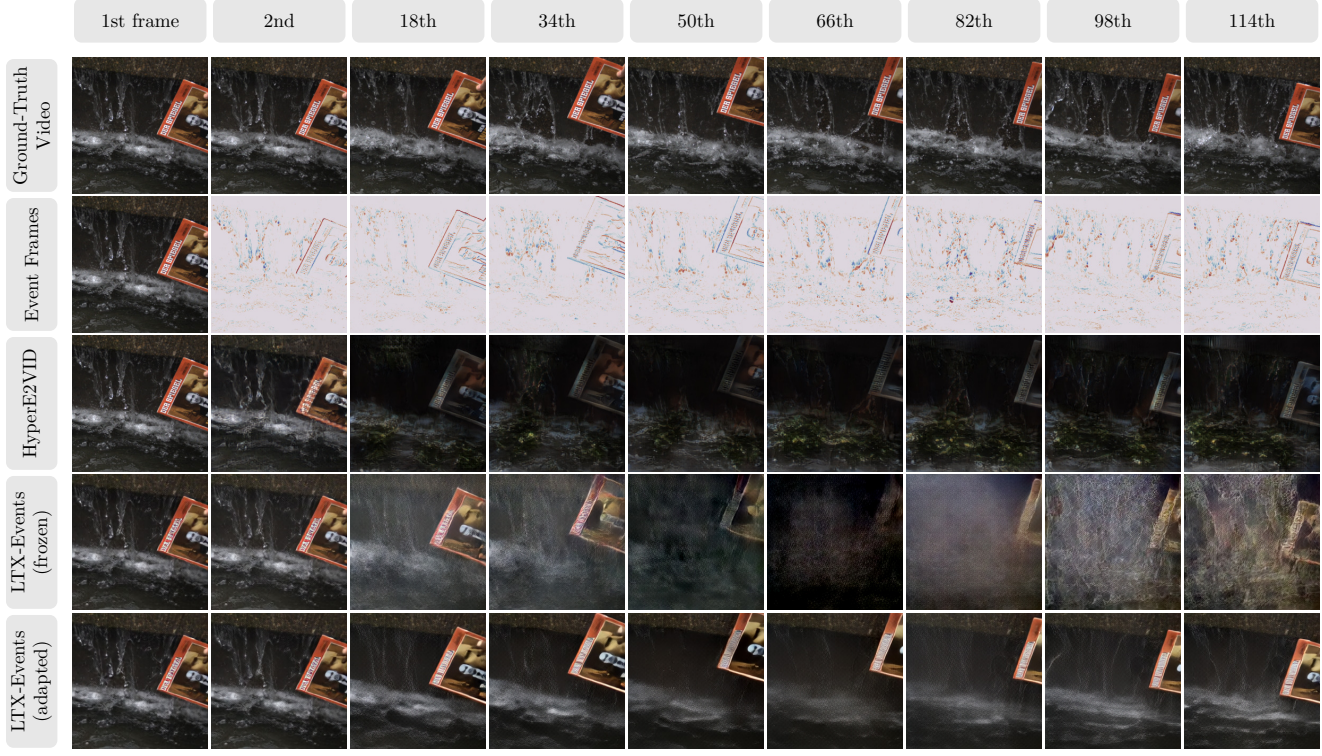


Figure 14. Qualitative comparison on HS-ERGB close (128 frames) showing a person moving a magazine in front of a water fountain. Column labels indicate frame numbers.

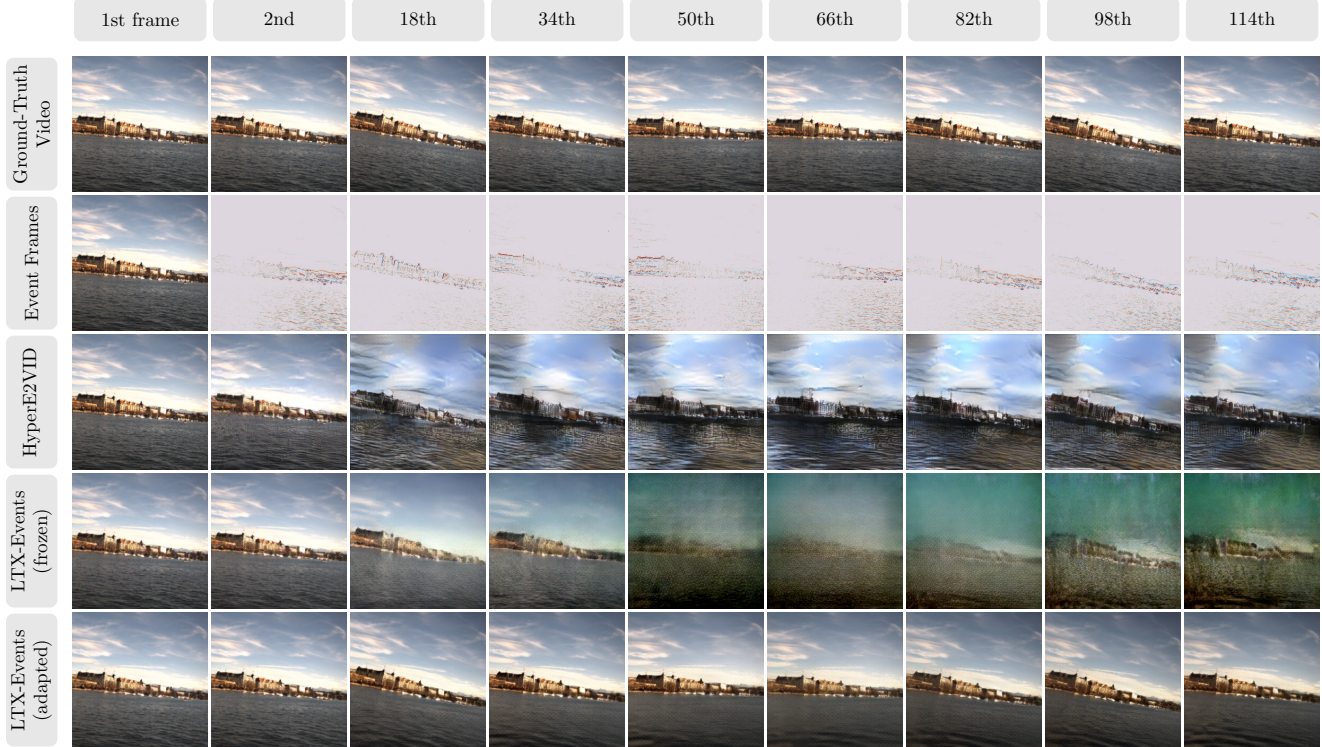


Figure 15. Qualitative comparison on HS-ERGB far (128 frames) showing egocentric camera motion in a far-field outdoor scene. Column labels indicate frame numbers.